IEEE Access
Multidisciplinary | Rapid Review | Open Access Journal

IEEE POWER & ENERGY SOCIETY SECTION

Received March 17, 2022, accepted April 23, 2022, date of publication April 26, 2022, date of current version May 4, 2022.

Digital Object Identifier 10.1109/ACCESS.2022.3170714

Systematic Evaluation of Photovoltaic MPPT Algorithms Using State-Space Models Under Different Dynamic Test Procedures

JOSE MIGUEL RIQUELME-DOMINGUEZ, (Graduate Student Member, IEEE), AND SERGIO MARTINEZ, (Senior Member, IEEE)

Department of Electrical Engineering, Escuela Técnica Superior de Ingenieros Industriales, Universidad Politécnica de Madrid, 28006 Madrid, Spain

Corresponding author: Sergio Martinez (sergio.martinez@upm.es)

This work was supported by the Spanish National Research Agency Agencia Estatal de Investigacion under Grant PID2019-108966RB-I00 /AEI/ 10.13039/501100011033.

ABSTRACT Maximum Power Point Tracking (MPPT) algorithms are essential in solar photovoltaic (PV) generation. In the last years, a major research effort has been made in order to get more efficient MPPT algorithms. However, in the literature, there is not a unique methodology for testing and comparing these kind of algorithms when facing dynamic irradiance conditions. This paper proposes a systematic way of evaluating and comparing MPPT algorithms for PV systems, at the simulation stage, unifying the following aspects: the PV system configuration, the type of simulation to be performed, and the dynamic irradiance tests to take into account. The MPPT algorithm is implemented into the dc-dc converter of the system for simplification purposes, simulations are carried out through state-space equations in order to reduce the total simulation time, and three irradiance dynamic tests are used systematically to provide full comparison under different environmental conditions. To test the flexibility of the proposed technique, a comparison of three commonly known Perturb and Observe (P&O) algorithms has been performed, giving special attention to the MPPT drift phenomenon. All interested researchers can request a computer application that implements the proposed methodology.

INDEX TERMS Dynamic test procedures, EN50530, MPPT drift, Perturb and Observe (P&O) algorithms, state-space model.

I. INTRODUCTION

Solar photovoltaics (PV) has been erected as the most promising energy source for modern power systems [1]. The need to reduce the carbon footprint and the availability of the solar resource are fundamental for the development of this technology. However, one of the biggest problems facing PV generation is that its power output highly depends on the environmental conditions, i.e. the incident solar irradiance and the PV cells temperature. Furthermore, the nonlinear characteristic of the P-V curve [2] hinders the optimum power extraction of solar energy when employing PV systems. As a consequence, all PV systems have to be equipped with a Maximum Power Point Tracking (MPPT) algorithm.

In the last two decades a great effort has been made to achieve more efficient MPPT algorithms. In fact, only between 2015 and 2020 more than 70 review papers have analyzed, discussed and compared different MPPT algorithms in terms of complexity, computational burden or implementation cost, among others [3]. Based on their operational principles [4], MPPT algorithms can be classified as follows: Hill Climbing methods, such as Perturb and Observe (P&O) [5], [6] and Incremental Conductance (IncC) [7], which take advantage from the form of the characteristic P-V curve; Fuzzy Logic Control (FLC) methods [8]–[10], which impose decision rules based on fuzzy levels [8]; Algorithms based on Curve Fitting [11], which estimate the characteristic curve and the position of the Maximum Power Point (MPP) in real-time via optimization techniques; MPP-locus methods [12], which assume the MPP lays on a straight line for different levels of irradiance; Beta-methods [13], [14], which apply a fixed-step size P&O when the operating point is near the MPP and a variable-step size P&O if it is far from the MPP. Table 1 summarizes the main MPPT methods

The associate editor coordinating the review of this manuscript and approving it for publication was Sarasij Das.

TABLE 1. Classification of photovoltaic MPPT algorithms based on their operational principles [4].

Algorithm	References	Strong Points	Drawbacks
Hill Climbing	[5]-[7]	Easy implementation Reduced cost	Steady-state oscillations MPPT Drift
Fuzzy Logic Control	[8]-[10]	Performance in variable conditions	Require extensive knowledge of the system
Curve fitting	[11]	High accuracy	Need for specific measurements
MPP Locus	[12]	Fast tracking speed	Insufficient tracking accuracy
Beta	[13]-[14]	Adaptive step size	Need for parameter tuning

that exist in the broader literature. It is important to mention that, although more complex MPPT algorithms are being developed, conventional methods like P&O and IncC still hold a major share of industrial applications [15].

After carefully reviewing the literature, a research gap has been detected, as there is no systematic methodology for developing, testing, and comparing MPPT algorithms to each other. This is critical in terms of time and economic consumption before experimental validation of the algorithms. In the literature, it is possible to find different PV system configurations based on single [16] or double stage converters [17]. However, when evaluating MPPT algorithms, just the dc-dc conversion stage is enough to test their adequacy. Another important aspect to define is the kind of simulation to be performed: traditional switching modeling approach or state-space modeling. The former has been widely used to date [18]- [19], although it is just limited to specific software such as MATLAB/Simulink or DIgSILENT/PowerFactory. The latter has been recently introduced in [20], with the advantage of applicability to any software or platform and reducing the computation time up to 300 times when compared to traditional switching modeling. However, [20] uses just one algorithm, the P&O one, and it is only examined using trapezoidal irradiance profiles.

Finally, the irradiance dynamic test procedure must be selected. In [21], three different dynamic tests have been identified: stepped dynamic test procedure [22], normalized EN50530 dynamic test procedure [23], and the day-by-day dynamic test procedure [24], although only the EN50530 test is carried out to analyze the performance of the fixed-step-size P&O algorithm (FS-P&O), the variable-step-size IC algorithm (VS-IC) and the hybrid-step-size beta method (HS-β), as it is recognized as the most cost-effective solution for the system. The three dynamic test procedures imply different considerations for their practical implementation. However, at the simulation stage, all of them can provide complementary information about performance of MPPT algorithms without the need to increase the complexity of the system or its cost.

This paper proposes a systematic evaluation of PV MPPT algorithms using a simplified version of the state-space model introduced in [20]. For simplification purposes, the PV system considered is formed by the PV array, the dc-dc converter and a voltage source in the place of the dc-link. In the proposed methodology, the three dynamic test procedures identified by [21] are implemented and used to provide a deep comparison in different environmental conditions. Three known P&O algorithms have been implemented and compared, particularly focusing on the MPPT drift phenomenon, namely: conventional P&O [5], Optimized MPPT for fast-changing environmental conditions (dP-P&O) [25], and Drift-Free Modified P&O (DF-P&O) [26]. Table 2 summarizes the novelties of the proposed methodology in contrast to [20] and [21]. The authors recently compared the above mentioned algorithms in [27] through traditional switching modeling and with real field irradiance conditions. This paper presents an extension of [27], being the main contributions described below:

TABLE 2. Comparison of the proposed methodology with the methods [20] and [21].

Method	Algorithms	Dynamic Tests	Methodology
[20]	P&O	EN50530	State-space
[21]	FS-P&O VS-IC HS-β	EN50530	Experimental
Proposed	P&O DF-P&O dP-P&O	Stepped EN50530 Day-by-day	Simplified State-space

1) A methodology for systematically evaluate the performance of PV MPPT algorithms is proposed. This procedure aims to unify the different simulation settings available in the literature.
2) A novel simplified state-space model is developed and particularized for three P&O algorithms (conventional P&O, DF-P&O, and dP-P&O) to reduce the computational burden of simulations.
3) The comparison between the algorithms is carried out with three different irradiance dynamic tests (stepped, EN50530 and day-by-day). This provides a deeper performance analysis of the algorithms in different environmental conditions.
4) All interested researchers can request a computer application that implements the proposed methodology.

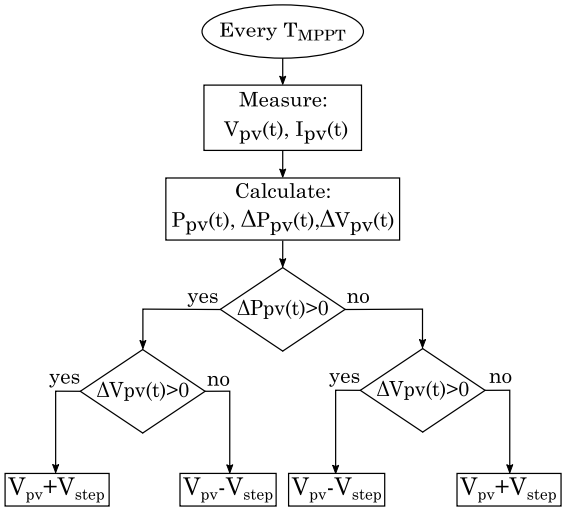

FIGURE 1. Flowchart of the conventional P&O algorithm.

Therefore, others may compare these P&O algorithms or even adapt the work to different MPPT algorithms.

The paper is organized as follows: Section II presents the conventional P&O algorithm and the MPPT drift phenomenon, Section III details the principle of operation of the dP-P&O and the DF-P&O algorithms, and Section IV introduces the dynamic test procedures. Section V develops the state-space models of the algorithms. In Section VI, simulation results are shown and, finally, Section VII draws conclusions of the work.

II. CONVENTIONAL PERTURB AND OBSERVE ALGORITHM AND MPPT DRIFT

Hill Climbing methods in general, and the conventional P&O algorithm [5] in particular, act on the principle of trial and error. While the PV system is operated at a reference voltage, every MPPT period, a perturbation V_{step} is deliberately applied to the reference voltage in order to observe the sign of the power variation. If the latter is positive, the next perturbation is applied in the same direction of the previous one. On the contrary, if the power variation is negative, the direction of the perturbation is reversed. As can be deduced, in steady-state environmental conditions, the PV system reaches the MPP and oscillates around it following the commonly known three-level operation. The flowchart of this algorithm is depicted in Fig. 1.

One of the main drawbacks of this algorithm manifests in situations of highly fluctuating irradiance. In these circumstances, the algorithm is not able to identify if an increment in PV power is due to the perturbation applied or caused by an increase in the incident irradiance. This undesired phenomenon, known as MPPT drift, is depicted in Fig. 2, where two power-voltage curves at different irradiance levels are plotted. In steady-state, with constant irradiance conditions, the normal operating sequence is $1-2-3-2-1$ indefinitely. However, let us suppose that when the operating point is

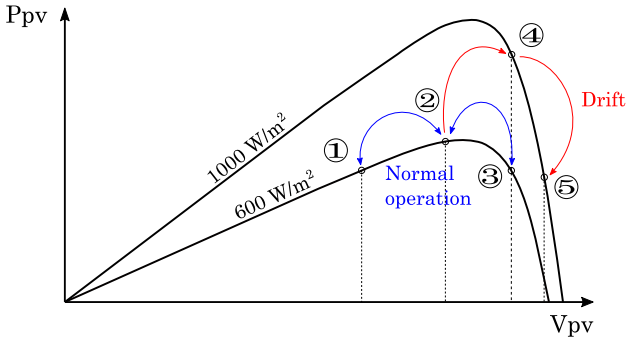

FIGURE 2. MPPT drift phenomenon in conventional P&O algorithm.

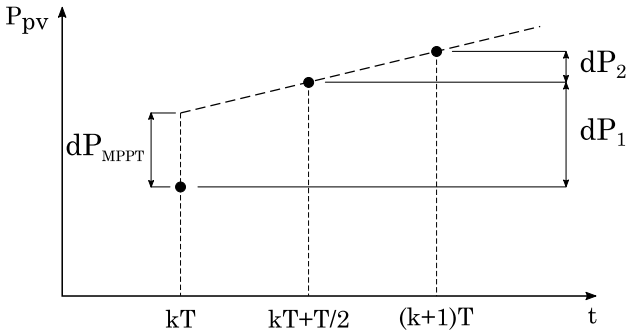

FIGURE 3. Explanation of the dP-P&O algorithm.

moving from 2 to 3 irradiance rises suddenly. Consequently, the operating point moves to 4. As the algorithm detects an increase in PV power, the following perturbation is applied in the same direction, so the final operation point is 5, producing power losses and instability. The next section presents two variants of the conventional P&O algorithm that try to avoid the MPPT drift phenomenon.

III. MODIFICATIONS OF THE CONVENTIONAL P&O ALGORITHM

This section presents two evolved versions of the conventional P&O, which try to avoid MPPT drift by incorporating additional power and current measurements.

A. OPTIMIZED MPPT FOR FAST-CHANGING ENVIRONMENTAL CONDITIONS (dP-P&O)

The dP-P&O algorithm is introduced in [25]. In contrast to the conventional P&O, this algorithm improves the assessment of the power variation by incorporating a new measurement in the middle of the MPPT period. In this way, it is possible to decouple the power variation caused by the perturbation applied and the one due to the irradiance change. Fig. 3 shows the operating principle of the dP-P&O algorithm.

The algorithm assumes that the PV system reaches the operating point during the first semi-period, i.e. from kT to $kT+T/2$. If this condition is satisfied, the power variation in the second semi-period dP_2, that is, from $kT+T/2$ to $(k+1)T$, is essentially due to the change in the incident irradiance. If the irradiance is assumed to vary constantly over the entire

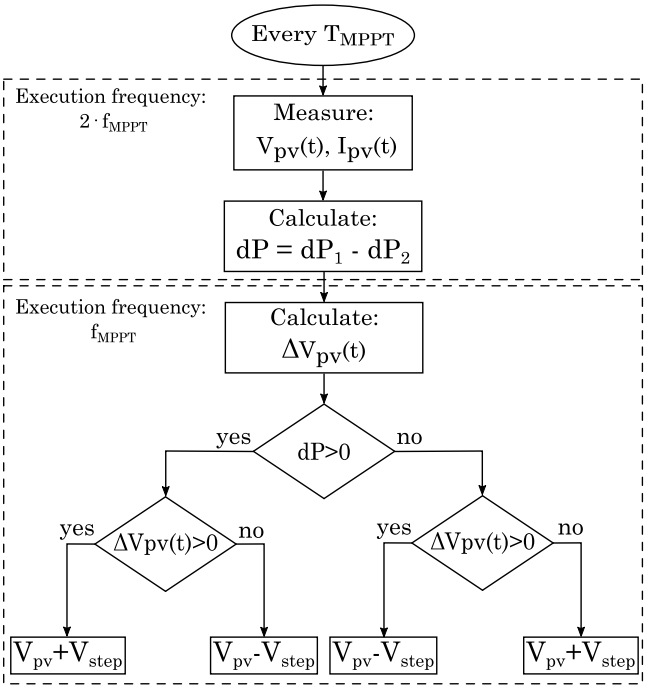

FIGURE 4. Flowchart of the dP-P&O algorithm.

MPPT period, the change in power due to the algorithm (dP_1) can be determined by (1). Fig. 4 depicts the steps followed by the dP-P&O algorithm.

$$dP_{MPPT} = dP_1 - dP_2 \tag{1}$$

B. DRIFT-FREE MODIFIED P&O ALGORITHM (DF-P&O)

The DF-P&O algorithm [26] is an evolved version of the conventional P&O which incorporates an additional verification of the PV current shift apart from the already mentioned power and voltage variations. This fact, together with the monotonically decreasing characteristic of the PV current-voltage curve, makes the identification of changes in the irradiance possible when the operating point moves to the right of the $I - V$ curve. When this happens, the direction of the disturbance applied is reversed. Fig. 5 depicts two current-voltage curves and the signs of the variables involved.

Let us consider that initially the operating point is 1. If, after the voltage disturbance, the operating point is 2, the voltage variation is positive and the current variation is negative, which is in accordance with the $I - V$ curve form and, therefore, the conclusion is that the irradiance remains constant. However, if the operating point moves to 3, both the voltage and current variations are positive, which imply that the incident irradiance has increased. The flowchart of the DF-P&O algorithm is shown in Fig. 6.

IV. MPPT DYNAMIC TEST PROCEDURES

This section details the differences between the dynamic test procedures identified in [21]. Although their implementation in an experimental setup can be laborious, at the simulation stage, each of these tests can provide supplementary information about the dynamic performance of MPPT algorithms.

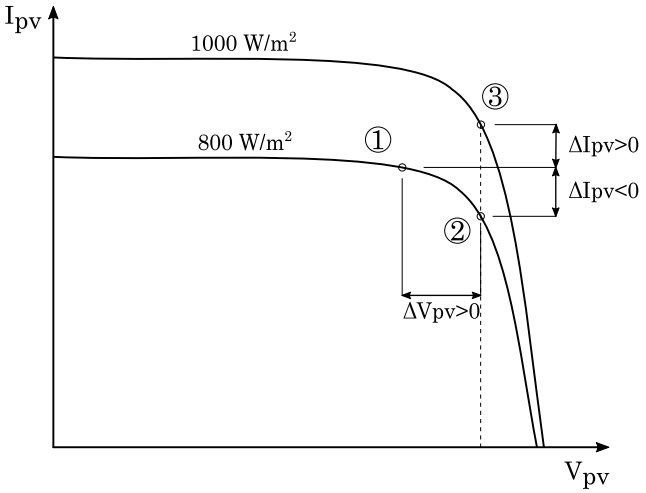

FIGURE 5. MPPT drift avoidance process.

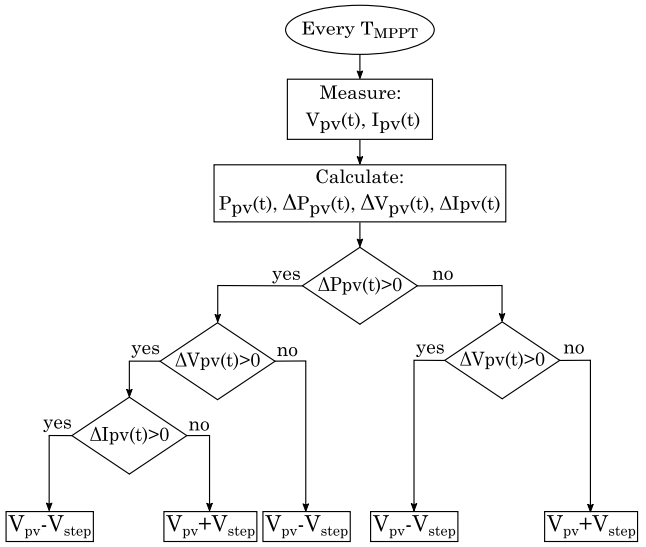

FIGURE 6. Flowchart of the DF-P&O algorithm.

TABLE 3. MPPT drift appearance in the stepped test.

Sub-period	1	2	3	4	5	6	7	8
Conv. P&O	yes	yes	no	no	yes	yes	no	no
dP-P&O	yes	no	no	no	yes	no	no	no
dF-P&O	yes	yes	no	no	no	no	no	no

A. STEPPED DYNAMIC TEST PROCEDURE

The stepped dynamic test is the simplest procedure to evaluate the performance of a MPPT algorithm. It considers that the incident irradiance in the PV system varies by means of steps. This method provides a first approximation to the effect of passing clouds above the PV system.

TABLE 4. Medium to high irradiance test (30% - 100% G_{STC}).

Nº of Repetitions	Ramp $W/(m^2\,s)$	Rise Time (s)	Dwell Time (s)	Down Time (s)	Dwell Time (s)	Total Time (s)
1	10	70	30	70	30	200
1	14	50	30	50	30	160
1	20	35	30	35	30	130
1	30	23	30	23	30	106
1	50	14	30	14	30	88
1	100	7	30	7	30	74

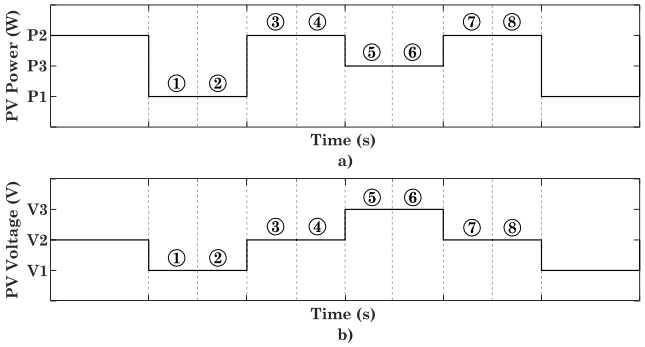

FIGURE 7. a) Power and b) voltage waveforms of P&O algorithms divided in sub-periods.

Despite its simplicity, this test allows for a clear visualization of the MPPT drift issue and for the identification of the causing mechanisms in each of the algorithms. Based on this test, in this section we propose a qualitative analysis for a preliminary study of the phenomenon under these irradiance conditions. It is constructed on the representation of power and voltage steady-state waveforms of the algorithms as presented in Fig. 7. These waveforms are commonly known as the three-level operation, as the operating point oscillates between three power-voltage coordinates.

As the MPPT drift situation depends on the instant at which the change in irradiance occurs, eight different sub-periods (1-8) can be considered as shown in Fig. 7. For example, when the conventional P&O is being used, a sudden increase in irradiance during sub-periods 1 or 2 could mislead the algorithm, making the total power variation to be positive ($\Delta P = P_1 - P_2$) when, in reality, the part of the variation due to the MPPT algorithm is negative. On the contrary, irradiance increments at sub-periods 3 or 4 don't affect the performance of the algorithm as $\Delta P = P_2 - P_1$ keeps its sign.

Table 3 summarizes the MPPT drift occurrences when irradiance increases by steps. It is worth noting that the change in irradiance must be large enough to produce MPPT drift. In this case, the conventional P&O suffers from MPPT drift in four of the eight sub-periods considered, as explained above. Compared to the conventional P&O, the dP-P&O reduces this probability by 50% due to the way that it measures the power variation (sub-periods 2 and 6). The same probability is achieved with the DF-P&O, in which the MPPT drift phenomenon is avoided at sub-periods 5 and 6 when compared to the conventional P&O.

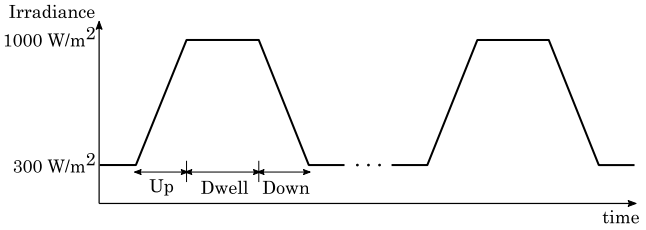

FIGURE 8. EN50530 ramp test (medium-high irradiance).

B. EN50530 DYNAMIC TEST PROCEDURE

The EN50530 dynamic test procedure is a globally accepted test for MPPT algorithms [28]. Different from the stepped dynamic test, standardized EN50530 is considered a more realistic approach for the MPPT dynamic performance evaluation. Specifically, it contemplates two synthetic trapezoidal irradiance profiles (low-medium and medium-high irradiance) that simulate the irradiation change under rapidly varying conditions. Figure 8 depicts the generic scheme of the EN50530 test procedure for the medium-high irradiance scenario.

As depicted, the irradiance profile starts at a medium irradiance level ($300\,W/m^2$). Then, during a certain time interval, there is an increase of the incident irradiance until it reaches a high level ($1000\,W/m^2$) and is maintained for a dwell time. Subsequently, irradiance is reduced at a constant rate to reach the initial value. In this paper, the medium-high irradiance scenario has been selected, with the parameters specified in Table 4.

C. DAY-BY-DAY TEST PROCEDURE

Compared to stepped and EN50530 tests, the day-by-day test procedure is the one that most approximates the real working conditions of the PV system and, therefore, it is more appropriate to test the dynamic performance of MPPT algorithms. However, the test bench requires long time to evaluate the dynamic performance of the MPPT. As an alternative, MPPT algorithms can be tested with real irradiance data that can be easily collected. In particular, this work considers irradiance data measured by National Resources Canada (NRCAN) [29] from two locations: Alderville and Varennes. As four different types of days were identified (clear sky, overcast, variable and very variable), data from the worst-case scenario will be used in order to test the dynamic performance of the

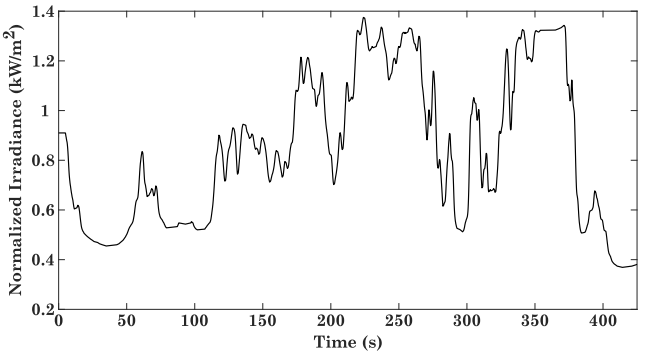

FIGURE 9. Irradiance data from Alderville in a very variable day.

MPPT algorithms. Figure 9 represents a four hundred second interval of this day.

It is worth noting that irradiance data have a high time resolution, with a sampling frequency up to 100 Hz, which makes them suitable for dynamic test studies.

V. STATE-SPACE MODEL OF THE PV SYSTEM

The evaluation of the already mentioned P&O algorithms requires a mathematical model that performs long simulations with minimal calculation burden. In this work, a simplified version of the state-space model described in [20] has been implemented. State-space representation is a widely used technique in modeling dynamic systems [30], [31]. In this representation, the system is characterized by state variables, which define the current state of the system. In addition, the system exchanges information with the outside environment through input and output signals. Input, output, and state variables are related by first-order differential and algebraic equations, in such a way that state variables change over time based on the values they hold at any given time and the values of input variables imposed externally. The values of output variables are determined exclusively by the values of state variables.

Figure 10 shows the electric circuit used, where the parasitic resistances of the capacitor (C_{in}), the boost converter and the DC-Link have been neglected. This assumption makes the capacitor voltage to match the terminal voltage of the PV array. The inputs, state variables, and the output have been highlighted with green, red, and blue colors respectively. It is worth noting that the proposed method assumes that the environmental conditions are the same for the entire PV array, i.e., the model is under uniform irradiance and temperature conditions. The PV array is modeled with its Single-Diode Model (SDM), whose implicit current-voltage relation is given by (2):

$$I_{pv} = I_{ph} - I_s \left[exp\left(\frac{V_{pv} + I_{pv} R_s}{V_T} \right) - 1 \right] - \frac{V_{pv} + I_{pv} R_s}{R_{sh}}, \tag{2}$$

where V_T is the thermal voltage of the P-N junction, described by (3):

$$V_T = \frac{n\,k\,T}{q} \tag{3}$$

TABLE 5. Main parameters of the PV system.

SDM parameters	I_{ph0}	$8.71\,A$	Boost converter	V_0	$350\,V$
	I_{s0}	$41.60\,nA$		C_{in}	$3.13\,\mu F$
	n_0	1.02		L	$36.63\,mH$
	R_{sh0}	$224.19\,\Omega$	PI controller	K_p	4.43×10^{-4}
	R_{s0}	$0.24\,\Omega$		K_i	0.89

where n is the ideality factor of the diode, k is the Boltzmann constant and q is the electron charge. Equation (2) can be rewritten in an explicit manner through the incorporation of the Lambert function (W):

$$I_{pv} = \frac{R_{sh}(I_{ph} + I_s) - V_{pv}}{R_s + R_{sh}} - \frac{V_T}{R_s} W \left[\frac{\frac{R_s R_{sh}}{R_s + R_{sh}} I_s exp\left(\frac{R_s R_{sh}(I_{ph}+I_s) + R_{sh} V_{pv}}{V_T (R_s + R_{sh})} \right)}{V_T} \right] \tag{4}$$

Table 5 lists the main parameters of the PV system composed of the PV array, the dc-dc boost converter and the PI controller.

De Soto *et al.* [32] developed the translation equations of the SDM parameters from Standard Test Conditions ($G_0 = 1000\,W/m^2, T_0 = 298.15\,K$) to the actual working conditions (G, T). In this work, just the variation of these parameters with the incident irradiance has been considered:

$$I_{ph} = \frac{G}{G_0} I_{ph0} \tag{5}$$

$$I_s = I_{s0} \tag{6}$$

$$n = n_0 \tag{7}$$

$$R_s = R_{s0} \tag{8}$$

$$R_{sh} = \frac{G_0}{G} R_{s0} \tag{9}$$

In [33], explicit equations were obtained to directly determine the MPP coordinates: V_{mp} and I_{mp}.

$$V_{mp} = \left(1 + \frac{R_s}{R_{sh}}\right) V_T\,(w - 1) - R_s\,I_{ph} \left(1 - \frac{1}{w}\right) \tag{10}$$

$$I_{mp} = I_{ph} \left(1 - \frac{1}{w}\right) - V_T \frac{(w - 1)}{R_{sh}} \tag{11}$$

where $w = W[I_{ph}\,e\,/I_s]$. Finally, the maximum available power can be computed as:

$$P_{mp} = V_{mp}\,I_{mp} \tag{12}$$

The average model of the boost converter is formed by the following differential equations (13)-(14), which determine the variation of the state variables (V_{pv} and i_L) over one switching period:

$$\frac{\partial V_{pv}}{\partial t} = \frac{I_{pv} - i_L}{C_{in}} \tag{13}$$

$$\frac{\partial i_L}{\partial t} = \frac{V_{pv} - (1 - D)V_o}{L} \tag{14}$$

The state-space model of the PI controller is described in equations (15)-(16), where ϕ is the state variable of the

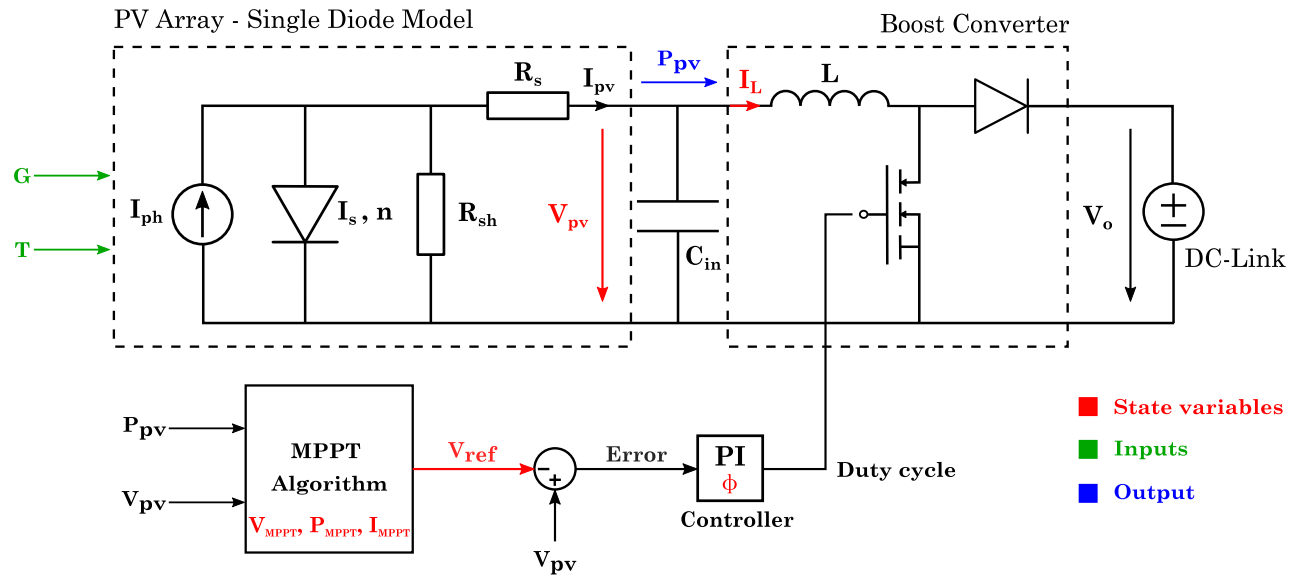

FIGURE 10. Electric circuit for the state-space model development.

controller and D is the duty cycle.

$$\frac{\partial \phi}{\partial t} = K_i(V_{pv} - V_{ref}) \tag{15}$$

$$D = \phi + K_p(V_{pv} - V_{ref}) \tag{16}$$

The complete state-space model is described by the state vector x, the input representing the environmental conditions u and the output of the model y (17)-(19):

$$x = [V_{pv} \ i_L \ \phi \ V_{ref} \ V_{MPPT} \ P_{MPPT} \ I_{MPPT}]^T \tag{17}$$

$$u = [G \ T]^T \tag{18}$$

$$y = P_{pv} \tag{19}$$

Continuous equations (13)-(15) can be discretized as (20)-(22). These equations update the state variables every sample time T_s.

$$V_{pv}^k = V_{pv}^{k-1} + \frac{I_{pv}^{k-1} - i_L^{k-1}}{C_{in}} T_s \tag{20}$$

$$i_L^k = i_L^{k-1} + \frac{V_{pv}^{k-1} - (1 - D^{k-1}V_o)}{L} T_s \tag{21}$$

$$\phi^k = \phi^{k-1} + K_i(V_{pv}^{k-1} - V_{ref}^{k-1})T_s \tag{22}$$

Finally, the model can be initialized with MPP conditions and the initial value of the duty cycle as:

$$D^o = 1 - \frac{V_{pv}^o}{V_o} \tag{23}$$

The state-space model of the P&O algorithms must be developed too. Next subsections present these models.

A. STATE-SPACE MODEL OF THE CONVENTIONAL P&O

The state-space model of the conventional P&O is described by (24)-(26): it comprises the update of the reference voltage and two state variables needed for the correct representation of the algorithm.

$$V_{ref}^k = \begin{cases} V_{ref}^{k-1} + sign\left(\dfrac{P_{pv}^{k-1} - P_{MPPT}^{k-1}}{V_{pv}^{k-1} - V_{MPPT}^{k-1}}\right) V_{step}, \\ \qquad if \ \ mod(kT_s, T_{MPPT}) = 0 \\ V_{ref}^{k-1}, \qquad otherwise \end{cases} \tag{24}$$

$$V_{MPPT}^k = \begin{cases} V_{pv}^{k-1}, & if \ \ mod(kT_s, T_{MPPT}) = 0 \\ V_{MPPT}^{k-1}, & otherwise \end{cases} \tag{25}$$

$$P_{MPPT}^k = \begin{cases} P_{pv}^{k-1}, & if \ \ mod(kT_s, T_{MPPT}) = 0 \\ P_{MPPT}^{k-1}, & otherwise \end{cases} \tag{26}$$

B. STATE-SPACE MODEL OF THE dP-P&O

The equations modeling the behaviour of the dP-P&O algorithm are (27)-(29). As previously mentioned in Section III A, the main novelty with respect to the conventional P&O is in the calculation of power variation.

$$V_{ref}^k = \begin{cases} V_{ref}^{k-1} + sign\left(\dfrac{dP^{k-1}}{V_{pv}^{k-1} - V_{MPPT}^{k-1}}\right) V_{step}, \\ \qquad if \ \ mod(kT_s, T_{MPPT}) = 0 \\ V_{ref}^{k-1}, \qquad otherwise \end{cases} \tag{27}$$

$$V_{MPPT}^k = \begin{cases} V_{pv}^{k-1}, & if \ \ mod(kT_s, T_{MPPT}) = 0 \\ V_{MPPT}^{k-1}, & otherwise \end{cases} \tag{28}$$

$$dP^k = \begin{cases} dP_1^{k-1} - dP_2^{k-1}, & if \ \ mod(kT_s, T_{MPPT}) = 0 \\ 0, & otherwise \end{cases} \tag{29}$$

C. STATE-SPACE MODEL OF THE DRIFT-FREE MODIFIED P&O

The state-space equations of the DF-P&O algorithm are defined by (30)-(33), with the incorporation of the PV current

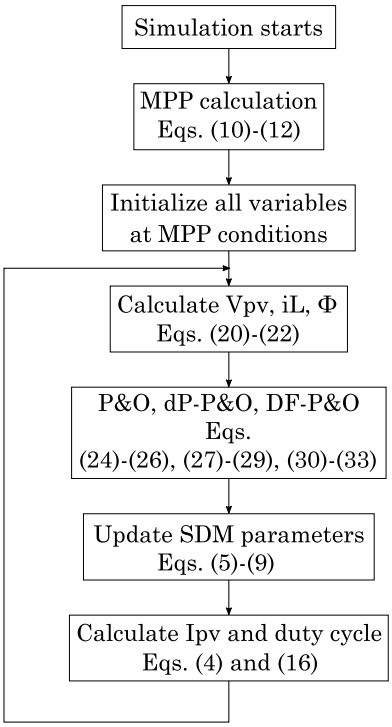

FIGURE 11. Flowchart of the proposed methodology.

variation in the algorithm decisions.

$$V_{ref}^{k} = \begin{cases} V_{ref}^{k-1} - sign(I_{pv}^{k-1} - I_{MPPT}^{k-1})V_{step}, \\ \quad if \;\; mod(kT_s, T_{MPPT}) = 0, \\ \quad \Delta V_{pv}^{k-1} > 0 \; and \; \Delta P_{pv}^{k-1} > 0 \\ V_{ref}^{k-1} + sign\left(\dfrac{P_{pv}^{k-1} - P_{MPPT}^{k-1}}{V_{pv}^{k-1} - V_{MPPT}^{k-1}}\right) V_{step}, \\ \quad elseif \;\; mod(kT_s, T_{MPPT}) = 0 \\ V_{ref}^{k-1}, \quad otherwise \end{cases} \tag{30}$$

where $\Delta V_{pv}^{k-1} = V_{pv}^{k-1} - V_{MPPT}^{k-1}$ and $\Delta P_{pv}^{k-1} = P_{pv}^{k-1} - P_{MPPT}^{k-1}$.

$$V_{MPPT}^{k} = \begin{cases} V_{pv}^{k-1}, & if \;\; mod(kT_s, T_{MPPT}) = 0 \\ V_{MPPT}^{k-1}, & otherwise \end{cases} \tag{31}$$

$$P_{MPPT}^{k} = \begin{cases} P_{pv}^{k-1}, & if \;\; mod(kT_s, T_{MPPT}) = 0 \\ P_{MPPT}^{k-1}, & otherwise \end{cases} \tag{32}$$

$$I_{MPPT}^{k} = \begin{cases} I_{pv}^{k-1}, & if \;\; mod(kT_s, T_{MPPT}) = 0 \\ I_{MPPT}^{k-1}, & otherwise \end{cases} \tag{33}$$

To sum up, Fig. 11 shows the steps followed by the methodology proposed. First, the MPP coordinates are determined and all the variables are initialized at those conditions. Then, the simulation loop starts and the mentioned equations have to be computed in the corresponding order. It can be seen that the methodology applied is common to all the three algorithms except for the way in which each one determines the reference voltage.

VI. SIMULATION RESULTS

The conventional P&O, the dP-P&O and the DF-P&O algorithms have been tested with the three dynamic test procedures detailed in Section IV. In order to quantify the effectiveness of the algorithms, the dynamic efficiency is used:

$$\eta_{dyn}(\%) = \frac{\int_o^{tf} P_{pv}\, dt}{\int_o^{tf} P_{MPP}\, dt} \times 100 \tag{34}$$

where tf is the final time of the simulation.

A. RESULTS OF THE STEPPED DYNAMIC SIMULATION

The three P&O algorithms have been tested with the Stepped Test Procedure. As previously discussed in Section IV, the MPPT drift depends on the instant that the irradiance change is produced. For this reason, a set of tests has been performed in which a known irradiance step is applied to the PV system and the response of the MPPT algorithm is recorded. Figure 12 shows the simulation results that correspond to the most critical situations, i.e., the sub-periods 1, 2, 5 and 6.

All the subplots in Fig. 12 depict the PV power (up) and PV voltage (down) evolution. Referring to the PV voltage response, it is possible to identify the three-level operation and the MPPT drift. As a consequence, there is a power loss that can be seen in the upper plot.

Figure 12 a) depicts the responses of the three algorithms when the irradiance change occurs in the first sub-period. As it is shown, all the mentioned algorithms show identical behaviour. A different conclusion can be drawn from Fig. 12 b), in which the step in irradiance happens at sub-period 2. This leads the conventional P&O and the DF-P&O to suffer from MPPT drift, while the dP-P&O can maintain the three-level operation. In terms of PV power, the power losses can be seen in the detailed zoom. In Fig. 12 c), the DF-P&O algorithm is the one that avoids the MPPT drift, whereas in Fig. 12 d) just the conventional P&O suffers from it.

In conclusion, the Stepped Test Procedure manifests that the moment at which the irradiance change occurs considerably affects the performance of the P&O algorithms. Due to their principle of operation, the dP-P&O and the DF-P&O algorithms reduce the probability of suffering from MPPT drift by 50% when compared to the conventional P&O. Analogous reasoning can be done for irradiance drops. Although the power losses are small when just a singular irradiance change is considered, as in this test, they can be relevant in situations with fluctuating irradiance conditions involving several ups and downs in short periods of time.

B. RESULTS OF THE EN50530 SIMULATION

The three P&O algorithms have been tested with the EN50530 dynamic test detailed in Table 1, which corresponds to the medium to high irradiance levels (30% - 100% G_{STC}). The parameters of the algorithms for this test are: $V_{step} = 1\,V$ and $F_{MPPT} = 0.5\,Hz$.

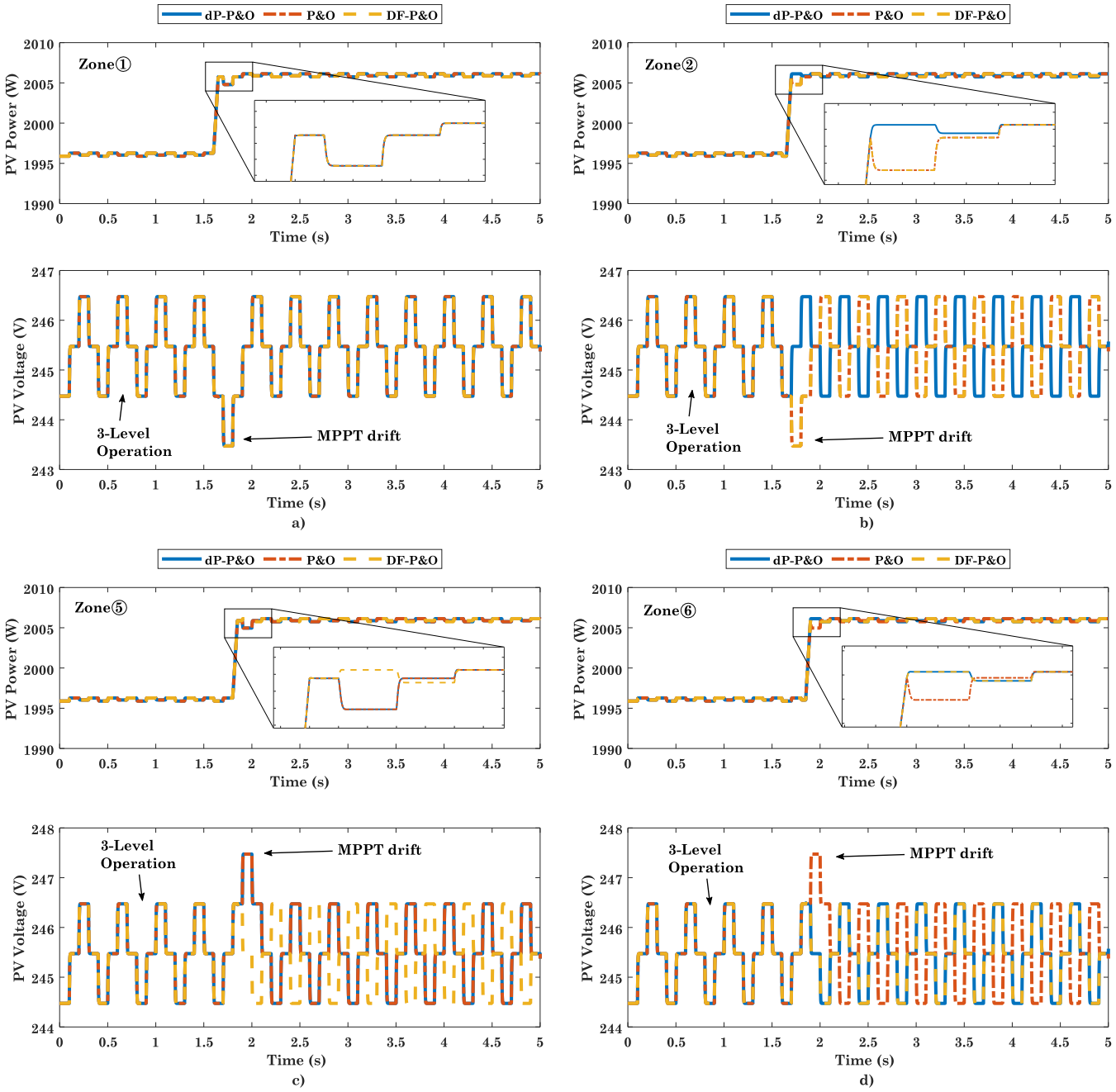

FIGURE 12. MPPT algorithms responses to the Stepped Test Procedure when the irradiance change is produced in: a) sub-period 1, b) sub-period 2, c) sub-period 5 and d) sub-period 6.

Figure 13 represents the results of the simulation. In Fig. 13 a), the PV power evolution is shown for the whole simulation. It can be seen that, for lower irradiance ramps, the MPPT drift is more severe for the conventional P&O and the DF-P&O, resulting in generation losses. Another perspective is shown in Fig. 13 b), where the evolution of PV voltage is represented. As depicted, the operating voltages deviate between algorithms due to their principles of operation.

Figures 13 c) and d) represent the trajectories of the operating points over the P-V curve for the zoomed parts of Figs. 13 a) and b). It can be seen that, in both cases, the three algorithms start close to the MPP but their trajectories are different. In particular, the DF-P&O and the conventional P&O suffer from MPPT drift as they deviate from V_{MPP}.

Table 6 shows the dynamic efficiency (equation 34) of the three algorithms in this test. As could be expected, the algorithm that best performs in the EN50530 test is the dP-P&O, with an efficiency close to 100%.

C. RESULTS OF THE DAY-BY-DAY SIMULATION

The day-by-day simulation has been performed with the data collected by NRCAN and detailed in Section IV c). The high temporal resolution of these data makes them suitable for

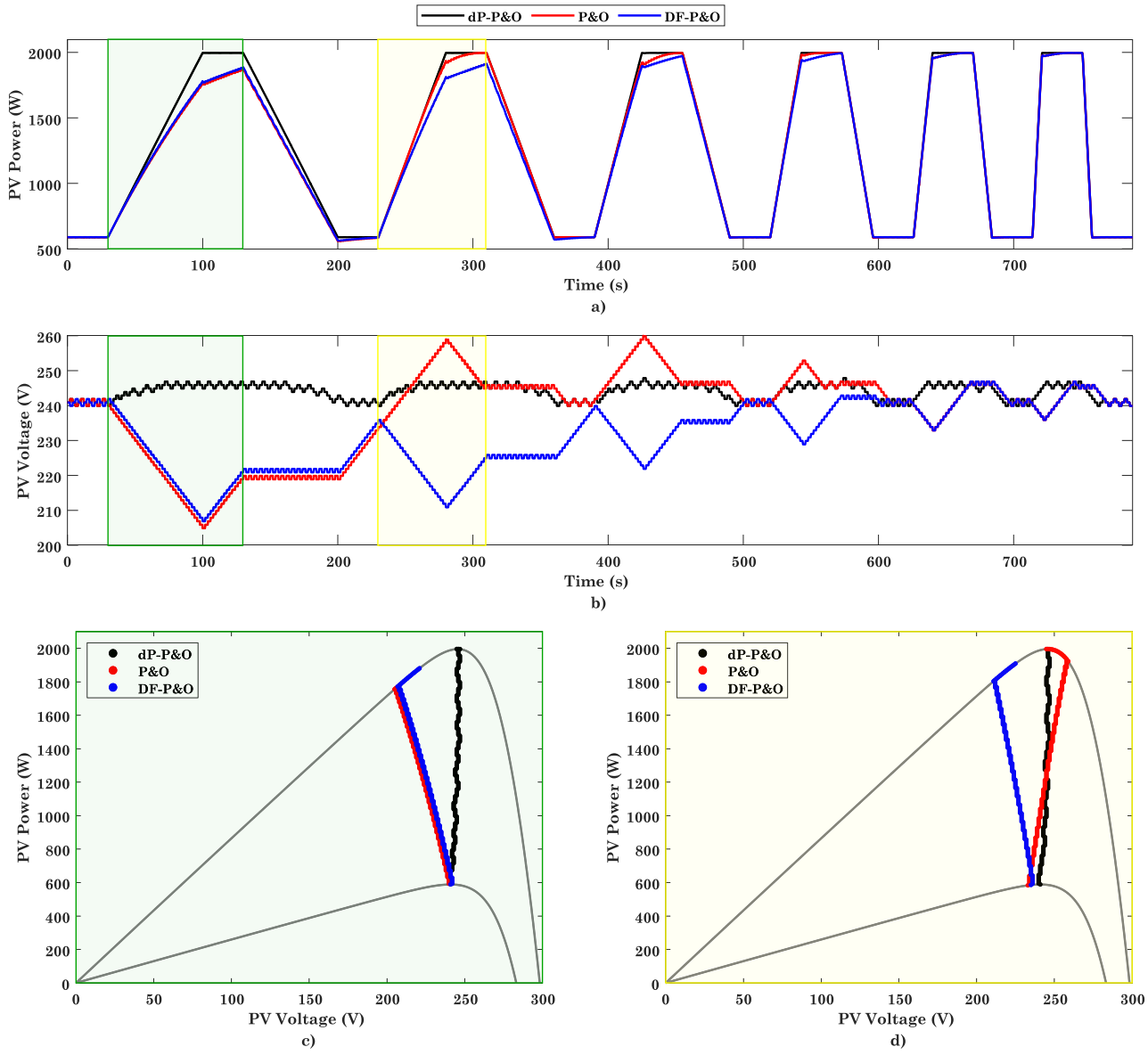

FIGURE 13. Simulation results of the Medium-High EN50530 irradiance test: a) PV power evolution, b) PV voltage evolution, c) and d) Trajectories over the P-V curve in the periods highlighted with green and yellow background, respectively.

TABLE 6. Dynamic efficiency of the EN50530 test.

Algorithm	$\eta_{dyn}(\%)$
Conventional P&O	97.87
Drift-Free P&O	96.77
dP-P&O	99.99

TABLE 7. Dynamic efficiency of the day-by-day test.

Algorithm	$\eta_{dyn}(\%)$
Conventional P&O	99.24
Drift-Free P&O	94.52
dP-P&O	99.99

evaluation of dynamic efficiency of MPPT algorithms. The parameters of the algorithms for this test are: $V_{step} = 1\,V$ and $F_{MPPT} = 10\,Hz$.

Figure 14 shows the results of the test. As depicted in Fig. 14 a), the power produced by the conventional P&O and the dP-P&O are similar, although in some instants (for example, at $t = 220$ and $t = 325$ seconds) the conventional P&O deviates from the MPP. However, the DF-P&O algorithm suffers from MPPT drift during the whole simulation, as it is confirmed in Fig. 14 b). It can be seen how the PV voltage is again deviated from the V_{MPP}.

Table 7 shows the dynamic efficiency obtained by the three algorithms. As analyzed, the efficiency of the conventional P&O is close to the one of the dP-P&O, which is the algorithm that clearly performs best in these circumstances. Again, the MPPT drift suffered by the DF-P&O algorithm penalizes its efficiency.

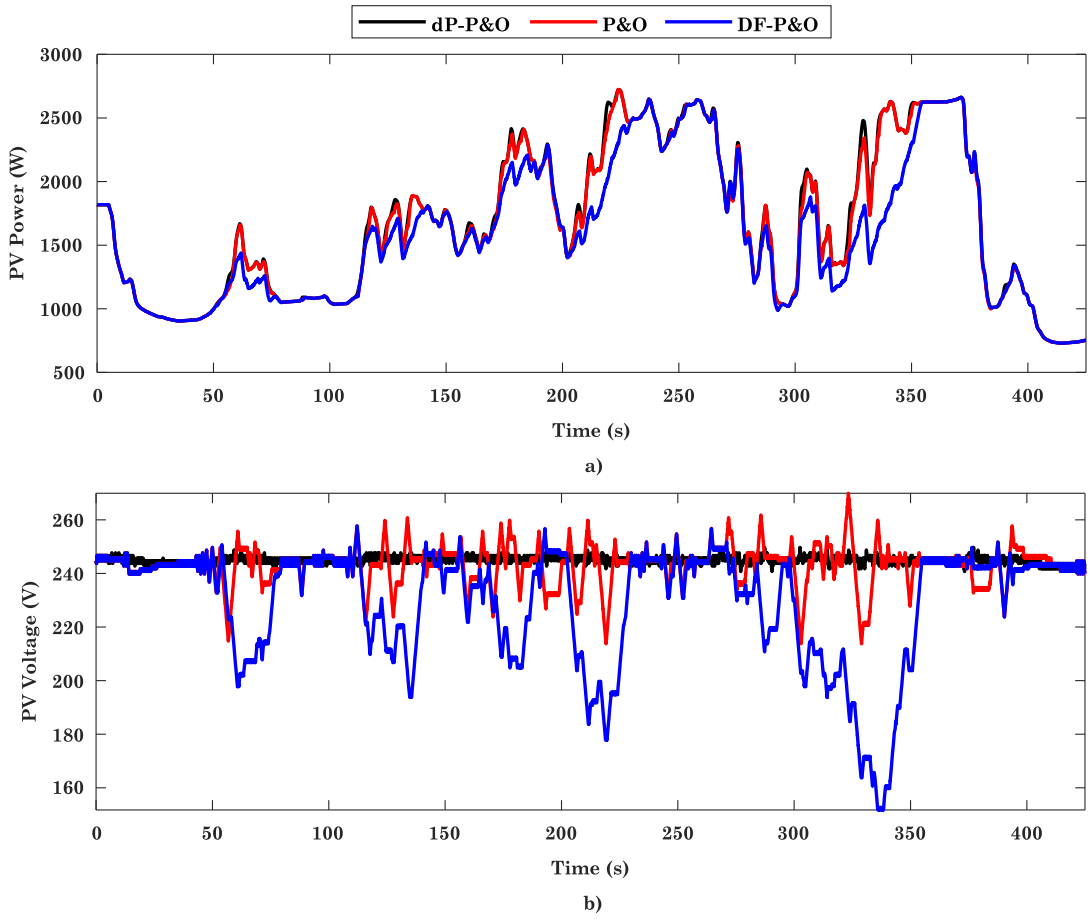

FIGURE 14. Simulation results of the day-by-day test.

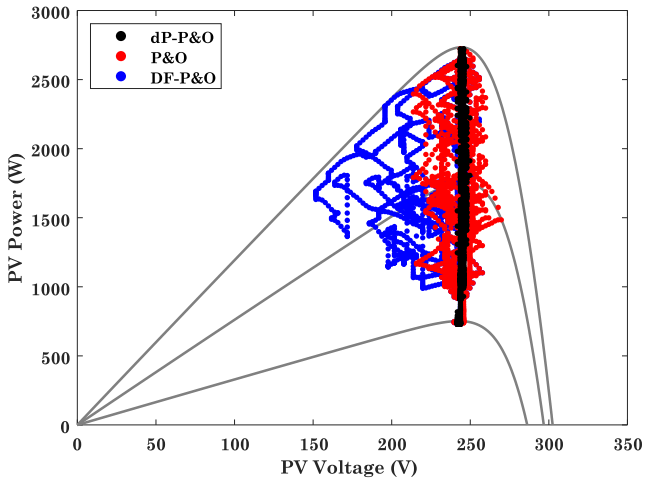

FIGURE 15. Operating point trajectories over the P-V curve for the day-by-day test.

Figure 15 shows the operating point trajectories over the P-V curve for this case. This plot is particularly interesting as it represents the movements of the algorithms along the whole simulation. As evidenced, the DF-P&O is the algorithm that most deviates from the MPP, followed by the conventional P&O and the dP-P&O algorithm, whose MPP track is almost perfect.

VII. CONCLUSION

In this paper, three known Perturb and Observe algorithms have been implemented through their state-space models. This development makes it possible to compare the performance of these algorithms in a wide range of tests, minimizing the calculation burden. For the performance evaluation, the three main MPPT dynamic tests have been considered: the stepped dynamic test, the EN50530 dynamic test and the Day-by-day test. In all of them, the dP-P&O is the one that obtains higher dynamic efficiencies, as simulation results show. These experiments show that the incorporation of an additional measurement of power in the middle of the MPPT period helps to avoid the MPPT drift in all conditions, with a minimal implementation cost.

The proposed methodology can be easily expanded to other MPPT algorithms, such as Beta or Fuzzy Logic methods, as well as other algorithms that may be developed in the future. Future studies may examine the possibility of incorporating the dc-ac inverter into the model, as well as adapting the presented model to partial shading conditions.

ACKNOWLEDGMENT

The authors would like to thank E. I. Batzelis from University of Southampton, for his help in explaining some implementation details of his work [20].

REFERENCES

[1] F. Aminifar, M. Shahidehpour, A. Alabdulwahab, A. Abusorrah, and Y. Al-Turki, "The proliferation of solar photovoltaics: Their impact on widespread deployment of electric vehicles," *IEEE Electrif. Mag.*, vol. 8, no. 3, pp. 79–91, Sep. 2020.

[2] I. F. Silva, P. D. S. Vicente, F. L. Tofoli, and E. M. Vicente, "Plotting characteristic curves of photovoltaic modules: A simple and portable approach," *IEEE Ind. Appl. Mag.*, vol. 27, no. 3, pp. 63–72, Feb. 2021.

[3] A. Ali, K. Almutairi, S. Padmanaban, V. Tirth, S. Algarni, K. Irshad, S. Islam, M. H. Zahir, M. Shafiullah, and M. Z. Malik, "Investigation of mppt techniques under uniform and non-uniform solar irradiation condition-a retrospection," *IEEE Access*, vol. 8, pp. 127368–127392, 2020.

[4] X. Li, Q. Wang, H. Wen, and W. Xiao, "Comprehensive studies on operational principles for maximum power point tracking in photovoltaic systems," *IEEE Access*, vol. 7, pp. 121407–121420, 2019.

[5] N. Femia, G. Petrone, G. Spagnuolo, and M. Vitelli, "Optimization of perturb and observe maximum power point tracking method," *IEEE Trans. Power Electron.*, vol. 20, no. 4, pp. 963–973, Jul. 2005.

[6] M. A. Elgendy, B. Zahawi, and D. J. Atkinson, "Operating characteristics of the P&O algorithm at high perturbation frequencies for standalone PV systems," *IEEE Trans. Energy Convers.*, vol. 30, no. 1, pp. 189–198, Mar. 2015.

[7] A. Safari and S. Mekhilef, "Simulation and hardware implementation of incremental conductance MPPT with direct control method using Cuk converter," *IEEE Trans. Ind. Electron.*, vol. 58, no. 4, pp. 1154–1161, Apr. 2011.

[8] B. N. Alajmi, K. H. Ahmed, S. J. Finney, and B. W. Williams, "Fuzzy-logic-control approach of a modified hill-climbing method for maximum power point in microgrid standalone photovoltaic system," *IEEE Trans. Power Electron.*, vol. 26, no. 4, pp. 1022–1030, Apr. 2011.

[9] X. Li, H. Wen, Y. Hu, and L. Jiang, "A novel beta parameter based fuzzy-logic controller for photovoltaic MPPT application," *Renew. Energy*, vol. 130, pp. 416–427, Jan. 2019.

[10] S. Tang, Y. Sun, Y. Chen, Y. Zhao, Y. Yang, and W. Szeto, "An enhanced MPPT method combining fractional-order and fuzzy logic control," *IEEE J. Photovolt.*, vol. 7, no. 2, pp. 640–650, Mar. 2017.

[11] J. M. Blanes, F. J. Toledo, S. Montero, and A. Garrigos, "In-site real-time photovoltaic I-V curves and maximum power point estimator," *IEEE Trans. Power Electron.*, vol. 28, no. 3, pp. 1234–1240, Mar. 2013.

[12] J.-C. Wang, Y.-L. Su, J.-C. Shieh, and J.-A. Jiang, "High-accuracy maximum power point estimation for photovoltaic arrays," *Sol. Energy Mat. Sol. Cells*, vol. 95, no. 3, pp. 843–851, 2011.

[13] M. A. G. de Brito, L. Galotto, L. P. Sampaio, G. E. de Azevedo e Melo, and C. A. Canesin, "Evaluation of the main MPPT techniques for photovoltaic applications," *IEEE Trans. Ind. Electron.*, vol. 60, no. 3, pp. 1156–1167, Mar. 2013.

[14] S. Jain and V. Agarwal, "Comparison of the performance of maximum power point tracking schemes applied to single-stage grid-connected photovoltaic systems," *IET Electr. Power Appl.*, vol. 1, no. 5, pp. 753–762, Sep. 2007.

[15] P. Bharadwaj and V. John, "Optimized global maximum power point tracking of photovoltaic systems based on rectangular power comparison," *IEEE Access*, vol. 9, pp. 53602–53616, 2021.

[16] B. Guo, M. Su, Y. Sun, H. Wang, B. Liu, X. Zhang, J. Pou, Y. Yang, and P. Davari, "Optimization design and control of single-stage single-phase PV inverters for MPPT improvement," *IEEE Trans. Power Electron.*, vol. 35, no. 12, pp. 13000–13016, Dec. 2020.

[17] M. N. Ali, K. Mahmoud, M. Lehtonen, and M. M. F. Darwish, "An efficient fuzzy-logic based variable-step incremental conductance mppt method for grid-connected pv systems," *IEEE Access*, vol. 9, pp. 26420–26430, 2021.

[18] M. J. E. Alam, K. M. Muttaqi, and D. Sutanto, "A multi-mode control strategy for VAr support by solar PV inverters in distribution networks," *IEEE Trans. Power Syst.*, vol. 30, no. 3, pp. 1316–1326, May 2015.

[19] V. N. Lal and S. N. Singh, "Control and performance analysis of a single-stage utility-scale grid-connected PV system," *IEEE Syst. J.* vol. 11, no. 3, pp. 1601–1611, Sep. 2017.

[20] E. I. Batzelis, G. Anagnostou, and B. C. Pal, "A state-space representation of irradiance-driven dynamics in two-stage photovoltaic systems," *IEEE J. Photovolt.*, vol. 8, no. 4, pp. 1119–1124, Jul. 2018.

[21] X. Li, H. Wen, Y. Hu, Y. Du, and Y. Yang, "A comparative study on photovoltaic MPPT algorithms under EN50530 dynamic test procedure," *IEEE Trans. Power Electron.*, vol. 36, no. 4, pp. 4153–4168, Apr. 2021.

[22] Y. Wang, Y. Li, and X. Ruan, "High-accuracy and fast-speed MPPT methods for PV string under partially shaded conditions," *IEEE Trans. Ind. Electron.*, vol. 63, no. 1, pp. 235–245, Jan. 2016.

[23] W. Xiao, H. H. Zeineldin, and P. Zhang, "Statistic and parallel testing procedure for evaluating maximum power point tracking algorithms of photovoltaic power systems," *IEEE J. Photovolt.*, vol. 3, no. 3, pp. 1062–1069, Jul. 2013.

[24] R. B. A. Koad, A. F. Zobaa, and A. El-Shahat, "A novel MPPT algorithm based on particle swarm optimization for photovoltaic systems," *IEEE Trans. Sustain. Energy*, vol. 8, no. 2, pp. 468–476, Apr. 2017.

[25] D. Sera, R. Teodorescu, J. Hantschel, and M. Knoll, "Optimized maximum power point tracker for fast-changing environmental conditions," *IEEE Trans. Ind. Electron.*, vol. 55, no. 7, pp. 2629–2637, Jul. 2008.

[26] M. Killi and S. Samanta, "Modified perturb and observe MPPT algorithm for drift avoidance in photovoltaic systems," *IEEE Trans. Ind. Electron.*, vol. 62, no. 9, pp. 5549–5559, Sep. 2015.

[27] J. M. Riquelme-Dominguez and S. Martinez, "Comparison of different photovoltaic perturb and observe algorithms for drift avoidance in fluctuating irradiance conditions," in *Proc. EEEIC*, 2020, pp. 1–5.

[28] M. Metry, M. B. Shadmand, R. S. Balog, and H. Abu-Rub, "MPPT of photovoltaic systems using sensorless current-based model predictive control," *IEEE Trans. Ind. Appl.*, vol. 53, no. 2, pp. 1157–1167, Mar./Apr. 2017.

[29] Natural Resources Canada. *High Resolution Solar Radiation Datasets*. [Online]. Available: https://www.nrcan.gc.ca/energy/renewable-electricity/solar-photovoltaic% /18409

[30] H. Wang, K. Jiang, M. Shahidehpour, and B. He, "Reduced-order state space model for dynamic phasors in active distribution networks," *IEEE Trans. Smart Grid*, vol. 11, no. 3, pp. 1928–1941, May 2020.

[31] M. Wang, Y. Mu, F. Li, H. Jia, X. Li, Q. Shi, and T. Jiang, "State space model of aggregated electric vehicles for frequency regulation," *IEEE Trans. Smart Grid*, vol. 11, no. 2, pp. 981–994, Mar. 2020.

[32] W. De Soto, S. A. Klein, and W. A. Beckman, "Improvement and validation of a model for photovoltaic array performance," *Solar Energy*, vol. 80, no. 1, pp. 78–88, 2006.

[33] E. I. Batzelis, G. E. Kampitsis, S. A. Papathanassiou, and S. N. Manias, "Direct MPP calculation in terms of the single-diode PV model parameters," *IEEE Trans. Energy Convers.*, vol. 30, no. 1, pp. 226–236, Mar. 2015.

JOSE MIGUEL RIQUELME-DOMINGUEZ (Graduate Student Member, IEEE) was born in Spain, in 1993. He received the degree in electrical engineering from the Universidad de Sevilla, Seville, Spain, in 2015. He is currently pursuing the Ph.D. degree with the Universidad Politécnica de Madrid, Madrid, Spain.

His employment experience included the Spanish Transmission System Operator, Red Eléctrica de España. Since 2018, he has been with the Department of Electrical Engineering, Escuela Técnica Superior de Ingenieros Industriales, Universidad Politécnica de Madrid, where he is currently an assistant Professor. His research interests include grid connected photovoltaic systems and power system stability and control.

SERGIO MARTINEZ (Senior Member, IEEE) was born in Spain, in 1969. He received the M.Sc. degree in industrial engineering and the Ph.D. degree in electrical engineering from the Universidad Politécnica de Madrid, Madrid, Spain, in 1993 and 2001, respectively.

He is currently an Associate Professor with the Department of Electrical Engineering, Escuela Técnica Superior de Ingenieros Industriales, Universidad Politécnica de Madrid. His research interests include electrical generation from renewable energy and the provision of ancillary services from electrical equipment connected to power systems through power electronics.